reactions

MDPI

Article

Influence of Nanoconfinement on the Hydrogen Release Processes from Sodium Alanate

Kenneth Tuul [1] and Rasmus Palm [2,*]

[1] Institute of Chemistry, University of Tartu, Ravila 14a, 50411 Tartu, Estonia; kenneth.tuul@ut.ee
[2] Department of Applied Physics, KTH Royal Institute of Technology, 10691 Stockholm, Sweden
* Correspondence: rasmus.palm@ut.ee

Abstract: Sodium alanate ($NaAlH_4$) is a prospective H_2 storage material for stationary and mobile applications, as $NaAlH_4$ contains 7.4 wt% of H_2, and it is possible to do multiple H_2 release and accumulation cycles. Nanoconfinement is a potential solution to enhance the H_2 release properties of $NaAlH_4$. To optimize the supporting material and the synthesis method used for the nanoconfinement of $NaAlH_4$, a better understanding of the influence of nanoconfinement on the H_2 release processes is necessary. Thus, the H_2 release from bulk, purely nanoconfined, and intermediate $NaAlH_4$ is measured at different temperature ramp rates, and the characteristic parameters for each hydrogen release process are determined. Activation energies for each process are determined using the Kissinger method, and the effect of nanoconfinement on the activation energies is analysed. The impact of nanoconfinement on the H_2 release processes from $NaAlH_4$ and the limitations of each process in case of bulk and nanoconfined $NaAlH_4$ are presented and discussed. Nanoconfinement of $NaAlH_4$ decreases activation energies of the initial reversible H_2 release steps to between 30 and 45 kJ mol^{-1} and increased the activation energy of the last irreversible H_2 release step to over 210 kJ mol^{-1}.

Keywords: H_2 storage; nanoconfinement; $NaAlH_4$; activation energy

Citation: Tuul, K.; Palm, R. Influence of Nanoconfinement on the Hydrogen Release Processes from Sodium Alanate. *Reactions* **2021**, *2*, 1–9. https://doi.org/10.3390/reactions2010001

Received: 7 December 2020
Accepted: 14 January 2021
Published: 18 January 2021

1. Introduction

Hydrogen is a potential energy carrier, as H_2 can be produced directly from water through electrolysis, H_2 can be directly converted into electrical energy with up to 60% efficiency with fuel cells, and the only by-product during conversion into electricity is water [1,2]. Thus, using H_2 to accumulate cheap electricity from renewable sources during high winds and/or intense solar radiation would help balance the power grid and be a viable alternative to electric battery cars. One of the hindrances to the application of a hydrogen-based energy economy is the lack of a cheap and safe hydrogen storage technology. The current commercial standard for hydrogen storage in mobile applications is storing hydrogen in pressurized tanks of up to 700 bar [3]. As the compression of H_2 to such pressures, p, consumes at least 10% [4] of the stored energy, such high pressures have inherent hazards, and even then, the H_2 energy density is only 1.31 kWh L^{-1} at 25 °C, alternative H_2 storage methods are of high interest.

The storage of hydrogen in a chemically bound form inside complex metal hydrides offers the advantage of high H_2 density, storage at ambient temperature, T, and p_{H2} = 1 bar, and potential cyclability through the application of p_{H2} [5]. One of the most promising complex metal hydrides for H_2 storage is sodium alanate ($NaAlH_4$), which incorporates 7.4 wt% of H_2. The release of H_2 from the bulk phase can be described through three decomposition steps (Equations (1)–(3)). The thermodynamical equilibrium T of decomposition (i.e., the release of H_2) for the first two decomposition reactions (Equations (1) and (2)) of $NaAlH_4$ are at comparatively low temperatures (80 and 150 °C, respectively) [6]. Alas, the release of H_2 from the bulk phase is kinetically limited in the solid phase, and thus, the first H_2 release step from bulk $NaAlH_4$ starts at 183 °C (Equation (1)) with the melting

of $NaAlH_4$. H_2 is released (from Equation (1) to Equation (3)) over a wide T range (Figure 1 and Reference [7]). The third H_2 release step (Equation (3)) is of no use for H_2 storage as the reverse reaction has not been achieved at p_{H2} and T feasible for current gas storage systems. Thus, the main problems of a $NaAlH_4$-based H_2 storage system are the high temperature of H_2 release caused by the kinetic limitation, the irreversibility of the third decomposition step (Equation (3)), and the segregation of decomposition products (Al, NaH, and Na_3AlH_6) into separate phases, which decreases the cycling lifetime of $NaAlH_4$-based H_2 storage systems.

$$3NaAlH_4(l) \rightarrow Na_3AlH_6(s) + 2Al(s) + 3H_2 \uparrow T_{start} = 183\ ^\circ C \quad (1)$$

$$Na_3AlH_6(s) \rightarrow 3NaH(s) + Al(s) + 1\frac{1}{2}H_2 \uparrow T_{start} = 235\ ^\circ C \quad (2)$$

$$3NaH(s) \rightarrow 3Na(l) + 1\frac{1}{2}H_2 \uparrow T_{start} = 270\ ^\circ C \quad (3)$$

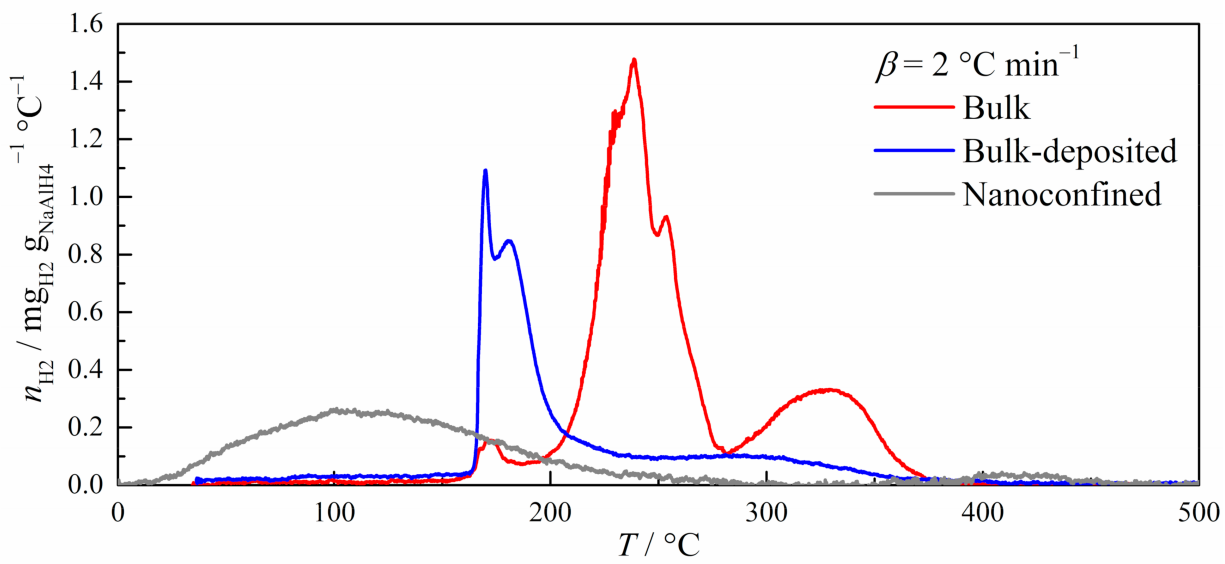

Figure 1. Hydrogen release curves of different forms of $NaAlH_4$ (noted in the figure) measured at a constant temperature ramp rate, β, of 2 °C min^{-1}.

The T of H_2 release from $NaAlH_4$ can be lowered through nanoscaling, where the higher surface area of sub-micrometer particles promotes the release of H_2 from $NaAlH_4$ at a T closer to that of thermodynamical equilibrium through the elimination of kinetical limitation present in case of bulk material, i.e., diffusion of H_2 inside the bulk phase. There are two main methods for nanoscaling $NaAlH_4$: reducing the average particle size through ball-milling or nanoconfining nanoscale particles unto a supporting porous material [7–11]. Whilst ball-milling is relatively easy to perform, and the T of H_2 release is considerably lowered during multiple hydrogenation/dehydrogenation cycles, the nanoscale particles agglomerate together at increased T, and the improved H_2 release properties are lost over multiple dehydrogenation/hydrogenation cycles [12]. By using a supporting porous material for nanoconfinement of $NaAlH_4$, the starting T of H_2 release is lowered to ambient conditions [8,13]. In addition, the agglomeration of $NaAlH_4$ and the segregation of decomposition products during dehydrogenation into separate phases is limited by the confinement of $NaAlH_4$, e.g., during dehydrogenation of bulk $NaAlH_4$, particles of Al form in the micrometer size. In contrast, the size of Al particles formed during the dehydrogenation of confined $NaAlH_4$ is lowered to tens of nanometers [13,14]. Nanoscale $NaAlH_4$ does not release H_2 according to Equations (1)–(3), where the direct decomposition of $NaAlH_4$ to NaH has been shown by Gao et al. [7], and the H_2 release curves are inherently

different, whereas the H_2 released from different decomposition steps (Equations (1)–(3)) from nanoconfined $NaAlH_4$ are visually inseparable [7,8,13].

To fine-tune the H_2 release properties of nanoconfined $NaAlH_4$, it is essential to understand the energetical barrier associated with each H_2 release step. It has been shown by Baldé et al. [8] that the decrease in $NaAlH_4$ particle size decreases the activation energy, E_a, of the decomposition process and is dependent on the particle size, where the E_a decreases from 116 kJ mol^{-1}, in the case of bulk material, to 58 kJ mol^{-1}, in the case of nanoparticles from 2 to 10 nm.

In this work, the influence of nanoconfinement on the H_2 release processes from $NaAlH_4$ is presented in depth. Bulk $NaAlH_4$, $NaAlH_4$ deposited as bulk material on a carbon support material, and completely nanoconfined $NaAlH_4$ materials are synthesized, and H_2 release curves at constant T ramp rates, $\beta = dT/dt$, are measured and analyzed. By comparing E_a values of H_2 release from different phases of $NaAlH_4$, i.e., bulk, deposited as bulk on a supporting material, and nanoconfined, a more complete picture of the effect of nanoconfinement on the H_2 release processes from $NaAlH_4$ is obtained and presented.

2. Materials and Methods

2.1. Synthesis of $NaAlH_4$/Carbon Composites

$NaAlH_4$ is deposited on a high surface area, specific surface area = 1840 m^2 g^{-1}, microporous, most pores with widths under 2 nm, and high porosity, pore volume = 0.82 cm^3 g^{-1}, dry carbon material RP-20 (Kuraray, Japan) through the solution impregnation method. Tetrahydrofuran, THF (anhydrous, ≥99.9%, Sigma-Aldrich, Germany), is used as the solvent, and a 0.05 g_{NaAlH_4} $mL_{THF}{}^{-1}$ solution is used for all samples. Bulk $NaAlH_4$ (90%, Sigma-Aldrich, Germany) was dissolved and filtrated through a glass microfiber filter (GF/B, Whatman, UK) to remove any insoluble impurities. Samples with 5, 60, and 100 mass% of deposited $NaAlH_4$ are synthesized to yield the nanoconfined, bulk-deposited, and bulk $NaAlH_4$, respectively, and are denominated as such. In the case of the bulk $NaAlH_4$ sample, recrystallization is performed at identical conditions to get rid of any impurities, but without the carbon support material. All syntheses, sample storage, and sample preparation for further analysis were performed in an Ar-filled (5.0, Linde) glovebox (MBraun LABmaster sp, Germany). A full description of the synthesis process and the characterization of the synthesized materials is provided in [13].

2.2. Temperature Controlled Decomposition

The H_2 release curves at constant β were measured with the Autochem 2950HP (Micromeritics, USA) chemisorption analyzer. The amount of released H_2 was determined with a thermal conductivity detector, where a 50 mL min^{-1} N_2 (6.0, Linde) gas flow was used as the carrier gas. β from 0.5 °C min^{-1} to 10 °C min^{-1} were applied. A full description of the sample preparation and measurement routine is brought in [13]. Data reduction, data analysis, and H_2 release peak fitting were performed with the OriginPro Version 2016 (OriginLab Corporation, Northampton, MA, USA) software.

3. Results

3.1. Hydrogen Release from $NaAlH_4$/Carbon Composites

The bulk, bulk-deposited, and nanoconfined $NaAlH_4$ exhibit distinct H_2 release curve shapes (Figure 1) in the case of all β used. In the case of the bulk $NaAlH_4$, a low amount of H_2 is released at ~170 °C, which is just under the T for melting of bulk $NaAlH_4$. The release of H_2 at ~170 °C is most likely the release of H_2 from the surface layer and defect sites, for which the melting T is lower, and thus, H_2 is released before the melting of the bulk phase. Starting from T = 200 °C, H_2 is released from the bulk of the material through the decomposition steps Equations (1) and (2), and at T > 280 °C H_2 is released from the last decomposition step, Equation (3). At T > 375 °C, all of the H_2 has been released as the material has been completely decomposed.

In the case of bulk-deposited $NaAlH_4$, a very low amount of H_2 is already released, starting at $T < 90$ °C. The T at which the initial H_2 release starts depends strongly on the β applied and is released at an almost constant rate. This H_2 release step is caused by the small amount of $NaAlH_4$ deposited in an amorphous state (highly polycrystalline structure) and/or as separate nanosized particles during the recrystallization process. Starting from $T = 165$ °C, a high amount of H_2 is released over a narrow T range and is followed by a high amount of released H_2 over a wide T range up to ~200 °C, after which a low amount of H_2 is released at a constant rate up to $T \sim 375$ °C. These three steps correspond to $NaAlH_4$ decomposition: Equation (1) from the surface, Equations (1) and (2) from bulk, and Equation (3), respectively. For a better deconvolution of the H_2 release from different decomposition steps and processes, the whole H_2 release curve has been fitted with distribution functions (presented in the next section).

In the case of nanoconfined $NaAlH_4$ H_2 release starts already at ambient conditions, $T < 23$ °C in case of all applied β. H_2 is mainly released at $T < 200$ °C, with the shape of the H_2 release curve strongly dependent on the applied β. In addition, a very low amount of H_2 is released at $T > 400$ °C, which is most likely H_2 released from the decomposition of NaH. Thus, deconvolution of the H_2 release peaks through fitting is necessary to understand the decomposition processes of nanoconfined $NaAlH_4$.

The amount of H_2 released, compared to the theoretical amount of H_2 in the $NaAlH_4$ of the sample, yields the H_2 content efficiency of the investigated materials. The average H_2 content efficiencies are ~100%, ~66%, and ~40% for bulk, bulk-deposited, and nanoconfined, respectively. Thus, the amount of recovered H_2 from $NaAlH_4$ decreases with the deposition process, especially with the nanoconfinement of $NaAlH_4$. The decrease in H_2 content efficiency is likely caused by the decomposition of $NaAlH_4$ during synthesis, where the step-by-step addition of $NaAlH_4$ in THF solution to the carbon support promotes the decomposition of $NaAlH_4$, especially at the initial addition steps where $NaAlH_4$ is deposited as nanosized particles. In addition, as the H_2 release from nanoconfined $NaAlH_4$ begins at ambient conditions, it is very likely that some of the nanoconfined $NaAlH_4$ decomposes during storage at ambient conditions, i.e., at 21 °C and in Ar gas environment.

3.2. Modelling of Decomposition Processes

To better understand the decomposition processes of $NaAlH_4$ in different phases, e.g., bulk, bulk-deposited, and nanoconfined, the H_2 release curves were fitted with a combination of gaussian and bigaussian peak functions (Figure 2). The bigaussian, i.e., an asymmetric gaussian profile distribution peak function which has two independent peak widths, w_1 and w_2, at $x < x_c$ (Equation (4)) and $x \geq x_c$ (Equation (5)), respectively, where x_c is the position of the peak center

$$y = y_0 + H \times \exp(-0.5 \times (x - x_c/w_1)^2) \text{ if } (x < x_c) \quad (4)$$

$$y = y_0 + H \times \exp(-0.5 \times (x - x_c/w_2)^2) \text{ if } (x \geq x_c) \quad (5)$$

where y_0 is the baseline and H is the peak height.

The bigaussian profile of the H_2 release is caused by the kinetic limitation of some decomposition steps, where the increase in the H_2 release amount with the initial rise in T is quick. After reaching maximum H_2 release from the process at temperature T_{max}, the H_2 release process continues over a wide T range as H_2 release from the decomposition process is kinetically hindered.

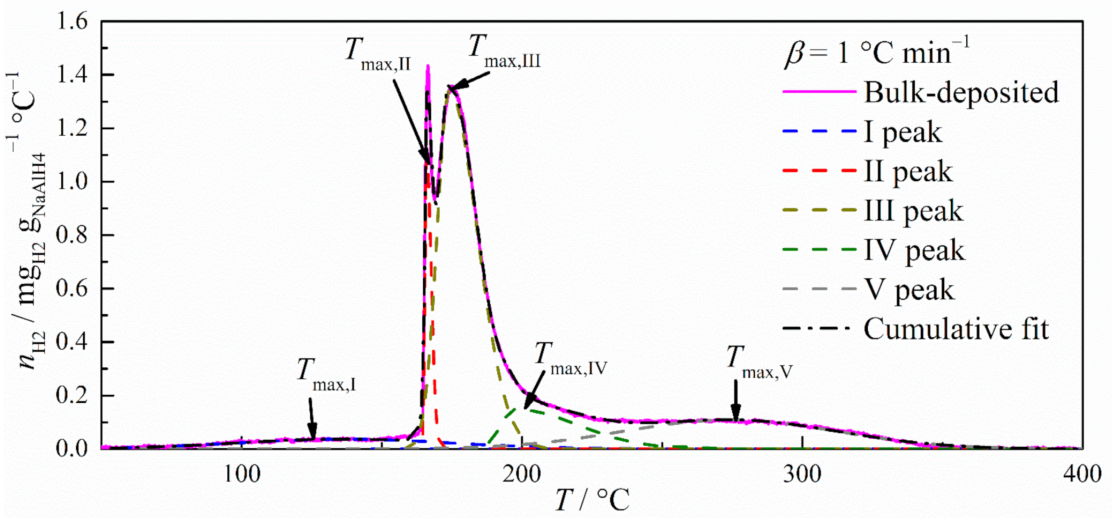

Figure 2. Hydrogen release curve from bulk-deposited measured during temperature ramp rate, β, of 1 °C min^{-1} with the corresponding hydrogen release peak fits.

From the fitting of the H_2 release curves, T_{max} is obtained for each decomposition process. The range of obtained T_{max}, determined from H_2 release curves measured at different β, is presented in Table 1 with the corresponding designations for each process. It is possible to calculate the E_a of a first-order reaction using the Kissinger method [8,15]

$$\ln(\beta/T_{max}^2) = \ln(Z \times R/E_a) - E_a/(R \times T_{max}), \quad (6)$$

where R is the ideal gas constant, and Z is the Arrhenius pre-exponential factor. By plotting $\ln(\beta/T_{max}^2)$ vs. $1/T_{max}$, the slope will yield $-E_a/R$, and thus, E_a can be calculated. The E_a values of the deconvoluted H_2 release processes have been calculated from the slope of the Kissinger plot (Figure 3, Table 1).

Table 1. Hydrogen release peaks and Kissinger method fitting results.

Material	Most likely H_2 Release step	Temperature Range of T_{max}/°C	E_a/kJ mol^{-1}	Additional Comments
Bulk	Equation (1)	167–172	–	Low amount, most likely only surface layer, no clear dependence of T_{max} on β
Bulk	Equation (1)	230–243	270 ± 10	Over a wide T range, from the whole phase
Bulk	Equation (2)	240–264	150 ± 60	Surface layer, low amount
Bulk	Equation (2)	245–279	120 ± 20	From the whole phase
Bulk	Equation (3)	308–337	150 ± 30	From the whole phase
Bulk-deposited	Equation (1)	129–165	–	Over a wide T range, no clear dependence of T_{max} on β. Most likely decomposition of nano- and surface layer.
Bulk-deposited	Equation (1)	165–174	400 ± 50	H_2 release over a very narrow T range
Bulk-deposited	Equation (1)	174–190	170 ± 20	From the whole phase
Bulk-deposited	Equation (2)	180–227	80 ± 10	From the whole phase
Bulk-deposited	Equation (3)	263–325	90 ± 20	From the whole phase
Nanoconfined	Equation (1)	51–57	70 ± 40	Only present at high β
Nanoconfined	Equations (1) and (2)	41–94	30 ± 5	Overlap strongly, both over a wide T range
Nanoconfined	Equations (1) and (2)	102–180	45 ± 5	
Nanoconfined	Equation (3)	407–452	210 ± 30	Low amount

In the case of bulk $NaAlH_4$, all the activation energies are relatively high, >100 kJ mol^{-1}, as the H_2 release processes are kinetically hindered by the diffusion of H_2 out of the bulk phase and by the thermal conductivity of the bulk phase, where the H_2 release processes from $NaAlH_4$ are endothermic [16], and thus preventively cooling the surrounding material upon decomposition. Even though the temperature of initial H_2 release from the first decomposition step depends on the applied constant β, the low amount of H_2 released hinders proper fitting. Thus, the obtained T_{max} does not remarkably depend on applied constant β. Therefore, the E_a could not be calculated and is most likely caused by the release of H_2 from the surface of $NaAlH_4$ particles over a wide range of T values under the melting T of bulk $NaAlH_4$. The highest E_a from the bulk material is for the second peak, which corresponds to Equation (1) reaction step from the bulk of the material. This H_2 release step is over a wide T range, as the H_2 diffusion length can vary widely in large $NaAlH_4$ particles, and thus H_2 release from inside the $NaAlH_4$ particles occurs at remarkably higher T values. Simultaneously with H_2 release from the Equation (1) reaction step, H_2 release from the Equation (2) reaction step starts. The H_2 release from the Equation (2) reaction step is discernably taking place in two distinct stages, as H_2 from the surface is released first, and then the H_2 from inside the particles is released. H_2 release from the last irreversible reaction step, Equation (3), is clearly separatable and has a relatively high E_a, 150 kJ mol^{-1}, as the decomposition products from preliminary H_2 release steps limit the kinetics of H_2 release from this step.

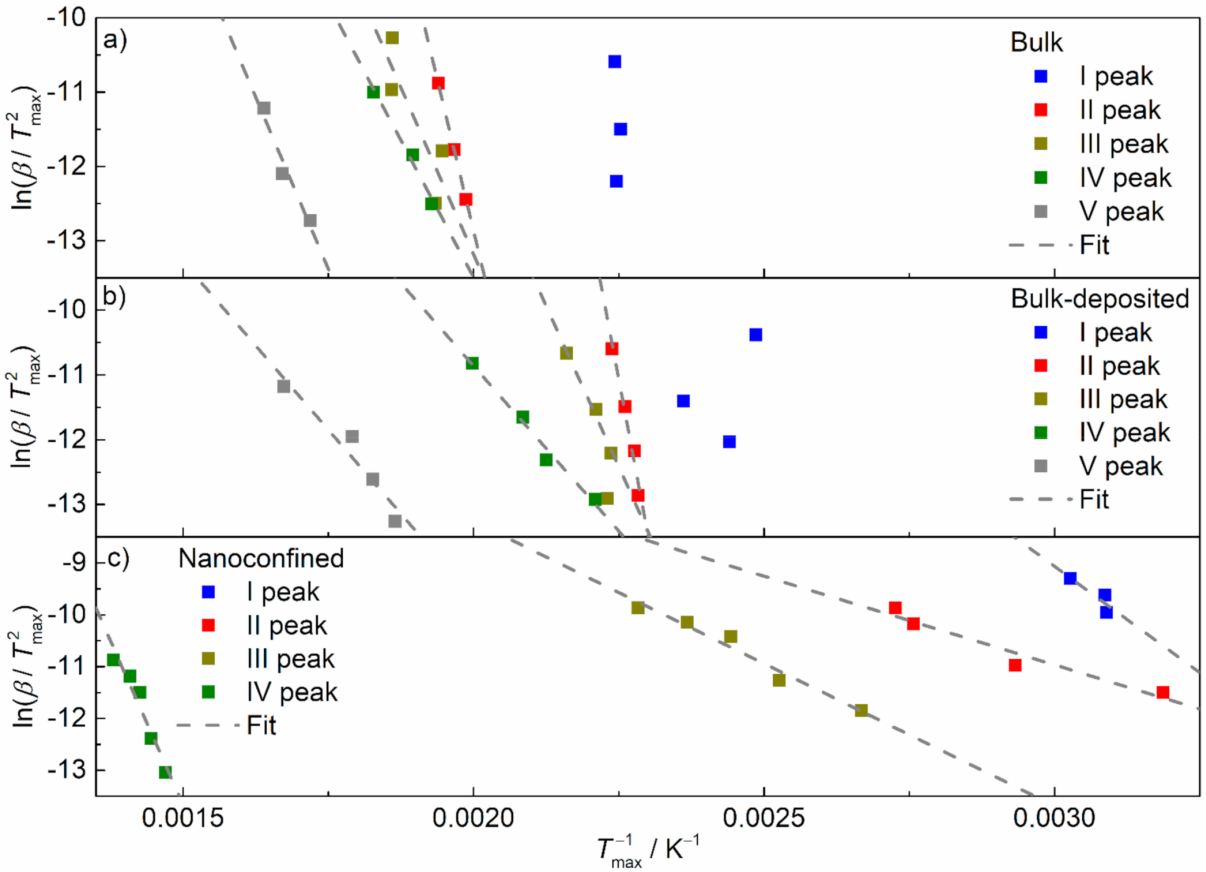

Figure 3. Kissinger equation plots of (**a**) bulk, (**b**) bulk-deposited, and (**c**) nanoconfined $NaAlH_4$ and the corresponding fits to the T_{max} of H_2 release processes obtained from fitting the H_2 release curves with gaussian and bigaussian peak functions.

A similar case can be seen for bulk-deposited, but the T_{max} of all H_2 release steps are lowered, and the E_a values of the last two steps are also lower. This is most likely caused by the partial confinement of the decomposition products inside the porous carbon structure, enhancing the kinetics of the H_2 release step corresponding to Equation (2). This restruc-

turing and the disappearance of clear crystalline phases upon the dehydrogenation of bulk-deposited $NaAlH_4$ has been shown before [10,13].

In the case of nanoconfined $NaAlH_4$, three separate H_2 release steps are identified under one continuous H_2 release peak, starting from ambient T and continuing up to 200 °C, where the H_2 release step starting with T_{max} from 51 to 57 °C is discernible only at a high applied constant β. All these H_2 release steps have relatively low E_a values, compared to bulk and bulk-deposited, are overlapping, and do not clearly correspond to a discrete H_2 release reaction. Baldé et al. have shown that the T_{max} of H_2 release decreases remarkably with the decrease in the nanoparticle size [8], and Gao et al. have shown that nanosized $NaAlH_4$ decomposes directly into NaH [7]. Thus, the indiscernibility of the H_2 release steps of nanoconfined $NaAlH_4$ is very likely caused by a distribution of differently sized $NaAlH_4$ nanoparticles, which decompose at different T values directly into NaH, going through the Equations (1) and (2) reactions in one step. In addition, the decomposition of the nanoconfined $NaAlH_4$ at ambient conditions, based on H_2 content efficiency, makes the assignment of the H_2 release peaks a nontrivial task. Regardless, the calculated E_a values, from 30 to 45 kJ mol^{-1}, of H_2 release steps discernible at all applied constant β from nanoconfined $NaAlH_4$ are notably lower than the value of 58 kJ mol^{-1} achieved for 2–10 nm $NaAlH_4$ particles [8]. The H_2 release step detected at the highest T, most likely from the Equation (3) reaction step, releases a low amount of H_2, and the T_{max} of this step is 100 °C higher than that of bulk and bulk-deposited materials and has an increased E_a. Thus, it is possible that nanoconfined $NaAlH_4$ does not decompose completely to Na and Al under the investigated conditions, as, for some reason, nanosized NaH is more stable than bulk NaH. This would improve the cyclability and usability of nanoconfined-$NaAlH_4$-based H_2 storage systems, as the decomposition of NaH is irreversible and, thus, unwelcome. The increased stability of the nanoconfined NaH phase must be investigated further.

The addition of fitting the H_2 release curves to deconvolute different decomposition steps before applying the Kissinger method has clearly shown that various activation barriers are present even in the case of nanoconfinement. This increases our understanding of the fundamental processes involved in releasing H_2 from $NaAlH_4$, especially when nanoconfined, which may prove vital when improving and optimizing such materials for H_2 storage applications.

The achieved activation energies for the reversible steps are considerably lower than most activation energies of mixed hydride [17–19], doped hydride [20–25], and nanoconfined hydride [9,26,27] systems described in the literature. Those include systems that utilize $NaAlH_4$ [9,19,24,25,27], but also other metal and complex hydrides [17,18,20–23,26]. Most activation energies for bulk hydrides are well over 100 kJ mol^{-1}. The achieved improved energies in the referred papers are mostly larger, by at least a factor of two, than the ones presented in this paper, with relatively few coming into the range of 30–45 kJ mol^{-1} [22,27]. This is remarkable, taking into account the simplicity of the system and its synthesis. Doping involves adding transition metals or compounds, which often adds a synthesis step of varying complexity. Mixtures may have side reactions, which are complex to analyze and may result in unwanted products or irreversible alloys [17–19]. Using a scaffold material for confinement improves cycling stability [13], which is essential for practical applications. In this work, the results have been achieved using a simple commercial microporous carbon, which offers lower E_a values than laboratory-made materials [26,27] and potentially higher loadings than, e.g., metal-organic frameworks [9]. Doping, ball-milling, and melt-infiltration, which even occurs naturally upon cycling above the melting temperature of $NaAlH_4$, is expected to improve the material's hydrogen storage properties even further.

4. Conclusions

The deconvolution of H_2 release processes through curve-fitting procedures to determine T_{max} when applying the Kissinger method significantly improved the amount and quality of the information received about the H_2 release processes in bulk, bulk-deposited,

and nanoconfined $NaAlH_4$. The coating of porous carbon particles with a thick layer of $NaAlH_4$, bulk-deposited, is shown to decrease the T_{max} of all H_2 release steps, whereas only the E_a values of the last steps are lowered. This indicates that whilst a supporting material reduces the T at which H_2 is released, the H_2 release processes are still limited by the H_2 diffusion out of the bulk phase. In the case of nanoconfined $NaAlH_4$, H_2 release starts at ambient T, and the E_a of H_2 release processes is remarkably lowered in comparison to bulk and bulk-deposited $NaAlH_4$. None of the H_2 release steps are limited by H_2 diffusion in the case of nanoconfined $NaAlH_4$. Even though the nanoconfined $NaAlH_4$ did not have a discrete particle size, based on the discernability of multiple H_2 release steps, very low E_a values from 30 to 45 kJ mol^{-1} are determined. These E_a values are a significant improvement on the vast majority of previously used techniques for nanoconfinement. The H_2 release at ambient T and the very low E_a of the nanoconfined $NaAlH_4$, in addition to limiting the final, irreversible decomposition step, highlights the possible utility of nanoconfinement for the improvement of $NaAlH_4$-based H_2 storage materials, where the critical problem is synthesizing nanoconfined composites with a high total H_2 yield per mass and/or volume.

Author Contributions: Conceptualization, R.P.; methodology, R.P.; formal analysis, R.P., K.T.; investigation, R.P.; resources, R.P.; writing—original draft preparation, R.P.; writing—review and editing, K.T.; funding acquisition, R.P. All authors have read and agreed to the published version of the manuscript.

Funding: This research was supported by the EU through the European Regional Development Fund (Centers of Excellence, TK141 2014-2020.4.01.15-0011) and by the Estonian Research Council Grant, grant number PUTJD957.

Conflicts of Interest: The authors declare no conflict of interest.

References

1. Von Helmolt, R.; Eberle, U. Fuel cell vehicles: Status 2007. *J. Power Sources* **2007**, *165*, 833–843. [CrossRef]
2. Peighambardoust, S.; Rowshanzamir, S.; Amjadi, M. Review of the proton exchange membranes for fuel cell applications. *Int. J. Hydrogen Energy* **2010**, *35*, 9349–9384. [CrossRef]
3. Hua, T.Q.; Ahluwalia, R.; Peng, J.-K.; Kromer, M.; Lasher, S.; McKenney, K.; Law, K.; Sinha, J. Technical assessment of compressed hydrogen storage tank systems for automotive applications. *Int. J. Hydrogen Energy* **2011**, *36*, 3037–3049. [CrossRef]
4. Makridis, S.S. Hydrogen storage and compression. In *Methane and Hydrogen for Energy Storage*; Carriveau, R., Ting, D.S.-K., Eds.; Institution of Engineering and Technology: London, UK, 2016; pp. 1–28.
5. Schüth, F.; Bogdanović, B.; Felderhoff, M. Light metal hydrides and complex hydrides for hydrogen storage. *Chem. Commun.* **2004**, *20*, 2249–2258. [CrossRef] [PubMed]
6. Ke, X.; Tanaka, I. Decomposition reactions for$NaAlH_4$, Na_3AlH_6, and NaH: First-principles study. *Phys. Rev. B* **2005**, *71*, 024117. [CrossRef]
7. Gao, J.; Adelhelm, P.; Verkuijlen, M.H.W.; Rongeat, C.; Herrich, M.; Van Bentum, P.J.M.; Gutfleisch, O.; Kentgens, A.P.M.; De Jong, K.P.; De Jongh, P.E. Confinement of $NaAlH_4$ in Nanoporous Carbon: Impact on H_2 Release, Reversibility, and Thermodynamics. *J. Phys. Chem. C* **2010**, *114*, 4675–4682. [CrossRef]
8. Baldeé, C.P.; Hereijgers, B.P.C.; Bitter, J.H.; De Jong, K.P. Sodium Alanate Nanoparticles—Linking Size to Hydrogen Storage Properties. *J. Am. Chem. Soc.* **2008**, *130*, 6761–6765. [CrossRef]
9. Bhakta, R.K.; Maharrey, S.; Stavila, V.; Highley, A.; Alam, T.; Majzoub, E.; Allendorf, M. Thermodynamics and kinetics of $NaAlH_4$ nanocluster decomposition. *Phys. Chem. Chem. Phys.* **2012**, *14*, 8160–8169. [CrossRef]
10. Zheng, S.; Fang, F.; Zhou, G.; Chen, G.; Ouyang, L.; Zhu, M.; Sun, D. Hydrogen Storage Properties of Space-Confined $NaAlH_4$Nanoparticles in Ordered Mesoporous Silica. *Chem. Mater.* **2008**, *20*, 3954–3958. [CrossRef]
11. Bendyna, J.K.; Dyjak, S.; Notten, P.H. The influence of ball-milling time on the dehydrogenation properties of the $NaAlH_4$–MgH_2 composite. *Int. J. Hydrogen Energy* **2015**, *40*, 4200–4206. [CrossRef]
12. Andrei, C.; Walmsley, J.C.; Brinks, H.; Holmestad, R.; Srinivasan, S.; Jensen, C.; Hauback, B. Electron-microscopy studies of $NaAlH_4$ with TiF3 additive: Hydrogen-cycling effects. *Appl. Phys. A* **2005**, *80*, 709–715. [CrossRef]
13. Palm, R.; Kurig, H.; Aruväli, J.; Lust, E. $NaAlH_4$ /microporous carbon composite materials for reversible hydrogen storage. *Microporous Mesoporous Mater.* **2018**, *264*, 8–12. [CrossRef]
14. Baldé, C.P.; Hereijgers, B.P.C.; Bitter, J.H.; De Jong, K.P. Facilitated Hydrogen Storage in $NaAlH_4$ Supported on Carbon Nanofibers. *Angew. Chem.* **2006**, *118*, 3581–3583. [CrossRef]
15. Blaine, R.L.; Kissinger, H.E. Homer Kissinger and the Kissinger equation. *Thermochim. Acta* **2012**, *540*, 1–6. [CrossRef]

16. Li, L.; Wang, Y.; Qiu, F.; Xu, Y.; An, C.; Jiao, L.; Yuan, H. Reversible hydrogen storage properties of $NaAlH_4$ enhanced with TiN catalyst. *J. Alloys Compd.* **2013**, *566*, 137–141. [CrossRef]
17. Shaw, L.L.; Ren, R.; Markmaitree, T.; Osborn, W. Effects of mechanical activation on dehydrogenation of the lithium amide and lithium hydride system. *J. Alloys Compd.* **2008**, *448*, 263–271. [CrossRef]
18. Xiong, Z.; Hu, J.; Wu, G.; Chen, P.; Luo, W.; Gross, K.; Wang, J. Thermodynamic and kinetic investigations of the hydrogen storage in the Li–Mg–N–H system. *J. Alloys Compd.* **2005**, *398*, 235–239. [CrossRef]
19. Ismail, M. Study on the hydrogen storage properties and reaction mechanism of $NaAlH_4$–MgH_2–$LiBH_4$ ternary-hydride system. *Int. J. Hydrogen Energy* **2014**, *39*, 8340–8346. [CrossRef]
20. Gu, J.; Gao, M.; Pan, H.; Liu, Y.-F.; Li, B.; Yang, Y.; Liang, C.; Fu, H.; Guo, Z.X. Improved hydrogen storage performance of $Ca(BH_4)_2$: A synergetic effect of porous morphology and in situ formed TiO_2. *Energy Environ. Sci.* **2012**, *6*, 847–858. [CrossRef]
21. Valentoni, A.; Mulas, G.; Enzo, S.; Garroni, S. Remarkable hydrogen storage properties of MgH_2 doped with VNbO5. *Phys. Chem. Chem. Phys.* **2018**, *20*, 4100–4108. [CrossRef]
22. Cui, J.; Wang, H.; Liu, J.; Ouyang, L.; Zhang, Q.; Sun, D.; Yao, X.; Zhu, M. Remarkable enhancement in dehydrogenation of MgH_2 by a nano-coating of multi-valence Ti-based catalysts. *J. Mater. Chem. A* **2013**, *1*, 5603–5611. [CrossRef]
23. Jangir, M.; Jain, A.; Yamaguchi, S.; Ichikawa, T.; Lal, C.; Jain, I. Catalytic effect of TiF_4 in improving hydrogen storage properties of MgH_2. *Int. J. Hydrogen Energy* **2016**, *41*, 14178–14183. [CrossRef]
24. Ali, N.; Ismail, M. Modification of $NaAlH_4$ properties using catalysts for solid-state hydrogen storage: A review. *Int. J. Hydrogen Energy* **2021**, *46*, 766–782. [CrossRef]
25. Sandrock, G.; Gross, K.; Thomas, G. Effect of Ti-catalyst content on the reversible hydrogen storage properties of the sodium alanates. *J. Alloys Compd.* **2002**, *339*, 299–308. [CrossRef]
26. Gross, A.F.; Vajo, J.J.; Van Atta, S.L.; Olson, G.L. Enhanced Hydrogen Storage Kinetics of $LiBH_4$ in Nanoporous Carbon Scaffolds. *J. Phys. Chem. C* **2008**, *112*, 5651–5657. [CrossRef]
27. Li, Y.; Zhou, G.; Fang, F.; Yu, X.Y.; A Zhang, Q.; Ouyang, L.Z.; Zhu, M.; Sun, D. De-/re-hydrogenation features of $NaAlH_4$ confined exclusively in nanopores. *Acta Mater.* **2011**, *59*, 1829–1838. [CrossRef]